Available online at www.sciencedirect.com

ScienceDirect

Journal of Magnesium and Alloys 12 (2024) 506–515

www.elsevier.com/locate/jma

Full Length Article

The growth of β phase in Mg-Gd-Y-Ni alloy by experimental and first-principles study

Yiqiang Hao[§], Lei Zhou[§], Zhiqing Chen, Zhixian Zhao, Bin Chen[*]

School of Materials Science and Engineering, Shanghai Jiao Tong University, 800 Dongchuan Road, Shanghai, 200240, China

Received 13 August 2021; received in revised form 20 October 2021; accepted 5 November 2021
Available online 13 December 2021

Abstract

The paper reports on the atomic investigation about β phase in $Mg_{96}Gd_2Y_1Ni_1$ alloy by using the first-principles study and the high-angle annular dark-field scanning transmission electron microscope (HAADF-STEM) corrected by atomic Cs. By using HAADF-STEM, the rectangular β phases were observed in the underage and peak aging stages in $Mg_{96}Gd_2Y_1Ni_1$ alloy. The β phase could be precipitated from the previously precipitated β phase, and the β phase grew in steps when it was precipitated. A special transition structure of three atomic layer thicknesses was first observed at the edge of the β phase and the structure of this interface is probably as the β/Mg_1 interface for the analysis of thermodynamic characterization and electronic characterization. The β' phase and the β_H structure were precipitated only at the edge of the length directions of the β phase. The β' phase continues to grow into a β phase directly without the formation of β_1 phase, resulting in an increase in the length of the β phase, which is discovered for the first time.

Keywords: HAADF-STEM; First-principles study; Mg-Gd-Y-Ni alloy; β phase; Growth; Interface.

1. Introduction

Magnesium alloys have been widely used in industry due to their low density, high specific strength and good recyclability [1]. However, the strength of the magnesium alloy is insufficient, especially the property of high-temperature strength, which limits its application. The addition of rare earth and transition metal elements to magnesium alloys can enhance the mechanical properties of magnesium alloys [2]. Especially the Mg-Gd-Y alloys have attracted much attention due to their high high-temperature strength and good creep resistance [3]. Researches on alloys such as Mg-Gd-Y-Mn and Mg-Gd-Y-Zn have been very thorough [4,5]. However, little is known about interfaces and growth trends of precipitated phases in the Mg-Gd-Y-TM (transition element: Ni, Mn or Zn) alloy.

In recent years, the atomic structure and aging precipitation sequence of magnesium alloys have been deeply explored by atomic resolution high angle annular dark-field scanning transmission electron microscopy (HAADF-STEM). The aging precipitation sequence of the Mg-Gd-Y alloy is reported to be: SSSS → GP zone (zigzag) → β'' (Mg_3Gd, hcp, DO19) → β' (Mg_7Gd, cbco) → β_1 (Mg_3Gd, fcc)→ β (Mg_5Gd, fcc) [6]. However, the β'' phase did not appear in the aging process in our previous studies [7]. What's more, there is scarcely atomic-scale study of the microstructure and growth of the β phase, like directly grown from the β' phase without the formation of the β_1 phase, which reveals a new growth of the β phase.

In this study, the atomic-scale Cs-corrected HAADF-STEM was used to characterize the microstructure and growth of the β phase precipitated during the aging of $Mg_{96}Gd_2Y_1Ni_1$ alloy. Moreover, the interface between β phase and Mg matrix along the growth direction is also analyzed by the first principle method. The results deepened our understanding of the microstructure and growth of the β phase.

* Corresponding author.
E-mail address: steelboy@sjtu.edu.cn (B. Chen).
§ L.Z and Y.H contributed equally.

https://doi.org/10.1016/j.jma.2021.11.015

2. Experimental procedures

In this experiment, the $Mg_{96}Gd_2Y_1Ni_1$ alloy (subscript represents the atomic ratio) was prepared from pure Mg (99.99%), pure Ni (99.99%), Mg-25 Y, and Mg-25 Gd master alloy (wt%). The solution treatment was carried out at 500°C for 8h, quenched in water at ~20 °C and then samples were isothermally aged at 200°C.

The samples for HAADF-STEM observation were prepared by the electrolytic twin-jet polishing using an electrolytic double sprayer model MTP-1A. Then the samples were polished and thinned by using Gatan's Precision Ion Polishing System II model 695. The HAADF-STEM characterization was proceeded on JEM-ARM200F, which was equipped with a Cs probe corretor and a cold field gun. The acceleration voltage was 200kV. The camera length was set to 8cm, resulting in a collection angle of 68-280 mrad.

3. Computational details

The lattice structure, stability and transformation process are calculated with the Vienna Ab initio Simulation Package (VASP) software which has the DFT framework [8,9] and projector augmented wave potentials [10]. The electronic characterization is calculated by CASTEP software [11]. The geometry optimizations of these precipitate structures were performed with exchange-correlation functional of the generalized gradient approximation (GGA) of the exchange-correlation potential in the form of Perdew-Burke-Ernzerhof (PBE) [12], which will cause the micro-displacement of atoms. The energy cut-off for the plane wave is 300 eV which is verified by the convergence test. The valence configurations are: Gd- 4f7 5s2 5p6 5d1 6s2, Mg- 2p6 3s2. The Brillouin zones are sampled with the k-point vectors of 2 × 2 × 1 for the bulk, which is also evaluated by the convergence test.

4. Experimental results and modeling

4.1. Experimental results

After the aging treatment of $Mg_{96}Gd_2Y_1Ni_1$ alloy for 4h and 53h, it is found that the rectangular β phases are precipitated in the magnesium matrix. The β phase is often present in as-cast alloys and, in addition, often appears as an equilibrium phase later in the aging stage. However, in this study, the β phase is present at the aged 4 h sample. The reason may be that the β phase already exists in the matrix at the very early stage according to Fig. 1(a)-(c) because of the insufficient solution and disperses in the matrix [13,14]. Then, the concentration of solute atoms at the grain boundary is much higher, resulting in a faster precipitation rate.

Fig. 1(a), (b) and (c) are HAADF-STEM images observed along the $[11\bar{2}0]_{Mg}$ direction of the as-cast, aged 4h and 53h samples, respectively, and it can be found that the β phases precipitate along the surface of cylinder precipitate. It can be seen from Fig. 1(b) that the β phases are staggered and are perpendicular to each other. Comparing Fig. 1(b) and (c), it can be found that the β phases in the aged 4h and 53h samples are all rectangular, but the β phases in the aged 53h sample are more elongated. In addition to this, there is a kind of blocky β phase with low contrast, but as the aging time increases, the shape and size don't change significantly due to the much larger volume of the β phase compared with other precipitate phases. After a rough statistical calculation, the average length of the β phase of Fig. 1(b) is 0.175 μm, and the average length of the β phase of Fig. 1(c) is 0.341 μm (In Fig. 1, only the lengths of the β phase of several typical lengths are indicated). The length of the β phase in the sample aged 53h sample is significantly increased. The change in width is negligible. It can be found from the study by Nie et al. that the more elongated cylindrical precipitate causes a greater increase in the critical resolved shear stress (CRSS), which leads to an increase in alloy strength [15].

It can be seen from Fig. 2(a) and Fig. 2(b) that the β phases are distributed in different directions. The atoms in the circle at A in Fig. 2(a) are enlarged to obtain Fig. 2(c). According to Fig. 2(c), the β phase having a lower luminance in the upper right corner is a new β phase that is precipitated from the β phase in the lower-left corner. The new β phase precipitates from the old β phase, and the direction changes. The angle of change is approximately 125° so that the β phases are dispersed in different directions in the alloy. It can be seen from Fig. 2(c) that there is a step between the new β phase and the old β phase, and it can be inferred that the new β phase grows in the step when it is precipitated.

The composition of the β phase with the Energy Dispersive Spectrometer (EDS) result (along the red in Fig. 2(a)) can be determined as Mg_5Gd. As in previous work [16], the β phase was determined to have a fcc structure, a lattice parameter of ~2.2 nm, and the orientation relationship of $(110)_\beta//[0001]_{Mg}$, $(\bar{1}12)_\beta//[1\bar{1}00]_{Mg}$ and $(1\bar{1}1)_\beta//[11\bar{2}0]_{Mg}$. For Fig. 2(c), the orientation relationship between β phase and Mg matrix is $(110)_\beta//[0001]_{Mg}$. The atomic model of Mg_5Gd observed along the $(110)_\beta$ direction is shown in the lower right corner of Fig. 2(c). The Mg atoms have been removed for convenience of observation. The number next to the Gd atoms represents the number of Gd atoms superimposed at this position. The higher the number of Gd atoms, the higher the brightness of the HAADF-STEM image.

The atoms in the circles at B in Fig. 2(b) are enlarged to obtain Fig. 2(d). There is an outwardly convex "step" on the left side of the β phase. The "step" is enlarged to obtain the HAADF-STEM image in the upper right corner of Fig. 2(d). If the solute atoms at the "step" continue to precipitate, a new β phase will precipitate.

Fig. 2(d) is further enlarged to obtain Fig. 2(e). As can be seen from Fig. 2(e), β' phase and β_H structure precipitate at the edge of β phase. Since the concentration of Gd atoms in the β phase is higher than the concentration of Gd atoms in the β' phase, the β' phase can precipitate from the β phase. There are atomic models of the β_H structure and β' phase (red atoms represent Gd atoms and yellow atoms represent magnesium atoms) in the upper right corner of Fig. 2(e). Zheng Jingxu et al. believed that the β_H structure was probably one

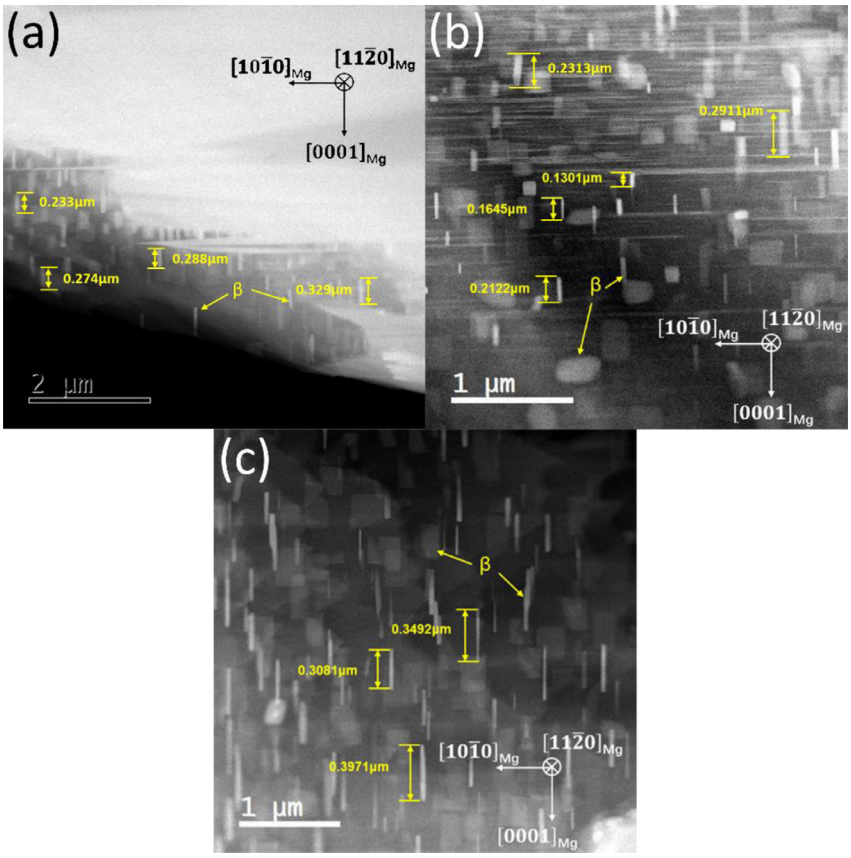

Fig. 1. (a), (b) and (c) show the distribution of β phase in the as-cast, 4 h and 53 h samples, respectively (observed along the $[11\bar{2}0]_{Mg}$ direction).

of the nucleation methods of precipitates, but it played a small role in the whole precipitation process [17]. According to the atoms marked by the yellow dotted frame in Fig. 2(e), it can be found that the atomic structures of the triangles and the parallelograms alternately appear at the edge of the β phase. The triangle consists of three Gd atoms, and the parallelogram consists of four Gd atoms. This special structure of the edge of the β phase has a thickness of approximately three atomic layers (0.66 nm). In order to reduce the interfacial energy, this special structure is formed at the boundary. This structure has not been reported so far.

Fig. 2(f) shows the β phase observed along the $[11\bar{2}0]_{Mg}$ direction. For Fig. 2(f), the orientation relationship between β phase and Mg matrix is $(1\bar{1}1)_{\beta}//[11\bar{2}0]_{Mg}$. The atomic model of Mg_5Gd observed along with the $(1\bar{1}1)_{\beta}$ direction is shown in the upper right corner of Fig. 2(f). There is a transition zone of about three atomic layer thicknesses between the β phase and the Mg matrix, and the thickness is 0.67 nm, which is marked with a yellow dotted frame in Fig. 2(f). This transition zone corresponds to the special structure at the edge of the β phase in Fig. 2(f).

The atoms at C in Fig. 2(b) are enlarged to obtain Fig. 2(g). Fig. 2(g) is similar to Fig. 2(e). It can be found that the β' phase and the β_H structure appear only at both ends of the β phase. Further, as can be seen from Fig. 1, as the aging time is extended, the β phase has only a significant change in length. It is speculated that the growth of the β phase is related to the β' phase. The β' phase is precipitated from both ends of the β phase, and then the β' phase grows into a β phase, whereby the length of the β phase increases.

To further prove that the β phase mainly grows along the length direction, the interface structure between the β phase and the Mg matrix is studied. According to Fig. 2(e), along the length extension direction of the β phase, the β phase is bordered by the long diagonal ($(1\bar{1}0)_{\beta}$) of the "parallelogram" structure marked by the blue lines in Fig. 3(a). According to Fig. 3(d), it can be found that only a small part of the magnesium atoms in the matrix are coherent with the magnesium atoms in the β phase. Along the length extension direction of the β phase, the lattice misfit of the β phase and the matrix is large, and the interface energy is high. Meanwhile, the nucleation and growth of precipitated phases easily occur in the energy concentration area, which provides the impetus for β' phase transition. Therefore, it's easy to precipitate the β' phase. According to Fig. 2(d), in the width direction of the β phase, the cross-section taken by the short diagonal ($(001)_{\beta}$) of the "parallelogram" structure (marked by the blue lines in Fig. 3(e)) intersects the substrate. According to Fig. 3(h), the matrix magnesium atom is semi-coherent with the magnesium atom in the β phase, the lattice misfit is small, the interface energy is low, the interface is relatively stable, and it is difficult to continue growing.

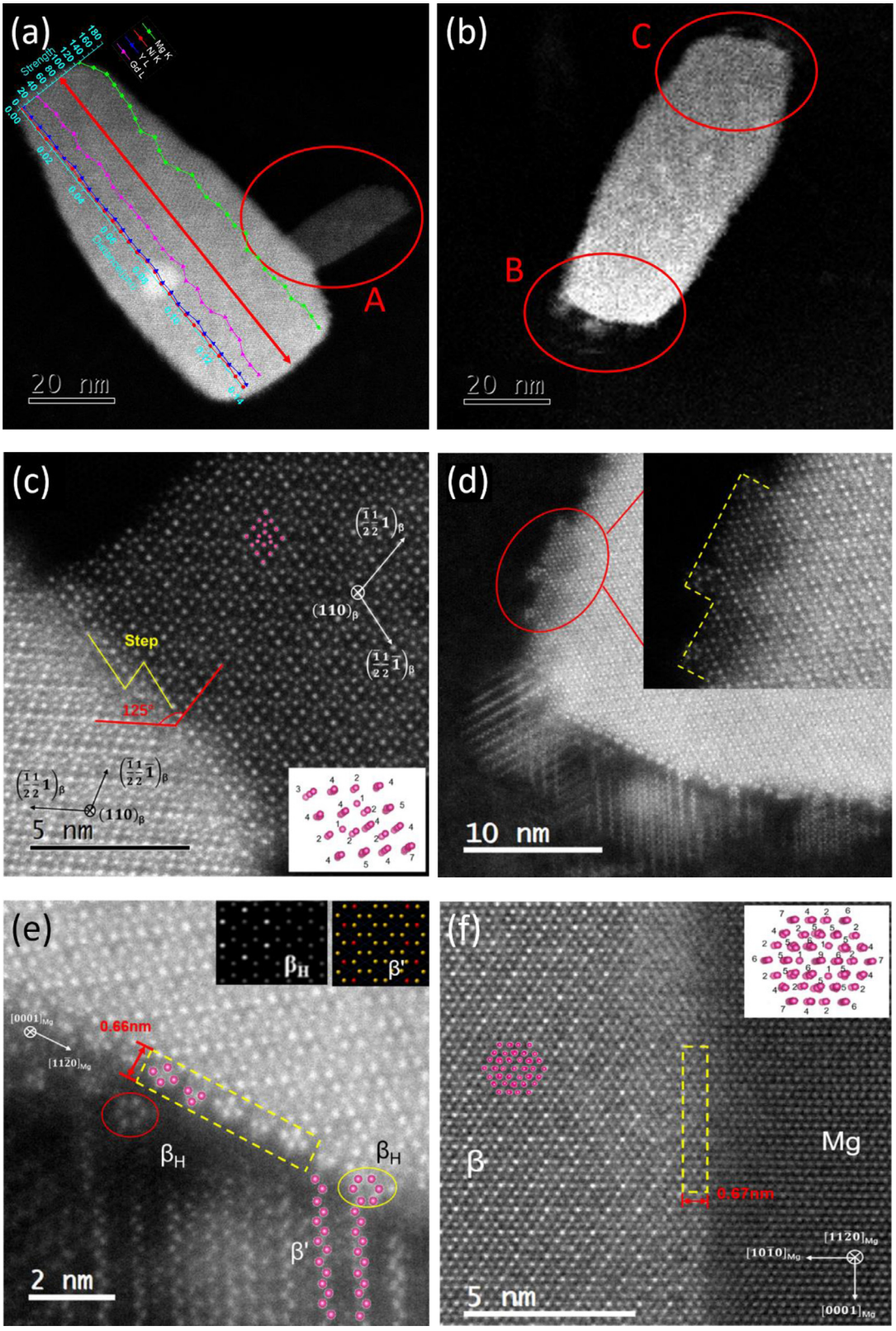

Fig. 2. (a) and (b) the β phases are distributed in different directions in the matrix and the EDS result of the phase β; (c) the new β phase precipitates from the old β phase, and the direction changes; (d) the new β phase extends directly from the old β phase to form a step; (e) and (g) the β' phase and the β_H structure are precipitated at both ends of the β phase; (f) β phase is observed along the surface of cylinder precipitate (4 h). ((a)–(e) and (g) are all observed along the $[0001]_{Mg}$ direction,(f) is observed along the $[11\bar{2}0]_{Mg}$ direction) (For interpretation of the references to color in this figure, the reader is referred to the web version of this article).

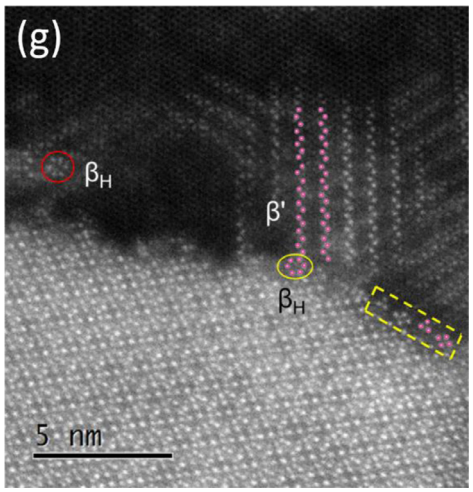

Fig. 2. Continued

4.2. The modeling procedure

Because it is hard to observe magnesium atoms accurately, there are 14 possible hypotheses of the β/Mg interface, which has different staggered positions shown in Fig. 4. The part of β interface is cut along $(1\bar{1}1)$, while the part of the Mg matrix is along $(11\bar{2}0)$. In Fig. 4(a), the Gd atoms in the Mg matrix are in the right part of the hexagonal structure, which is marked by a red square, as the β/Mg_1 interface. And the cluster of Gd atoms across the interface together form the combined structure of the rhombus and triangle, which is shown in Fig. 2(e). Analogously, the Gd atoms in the Mg

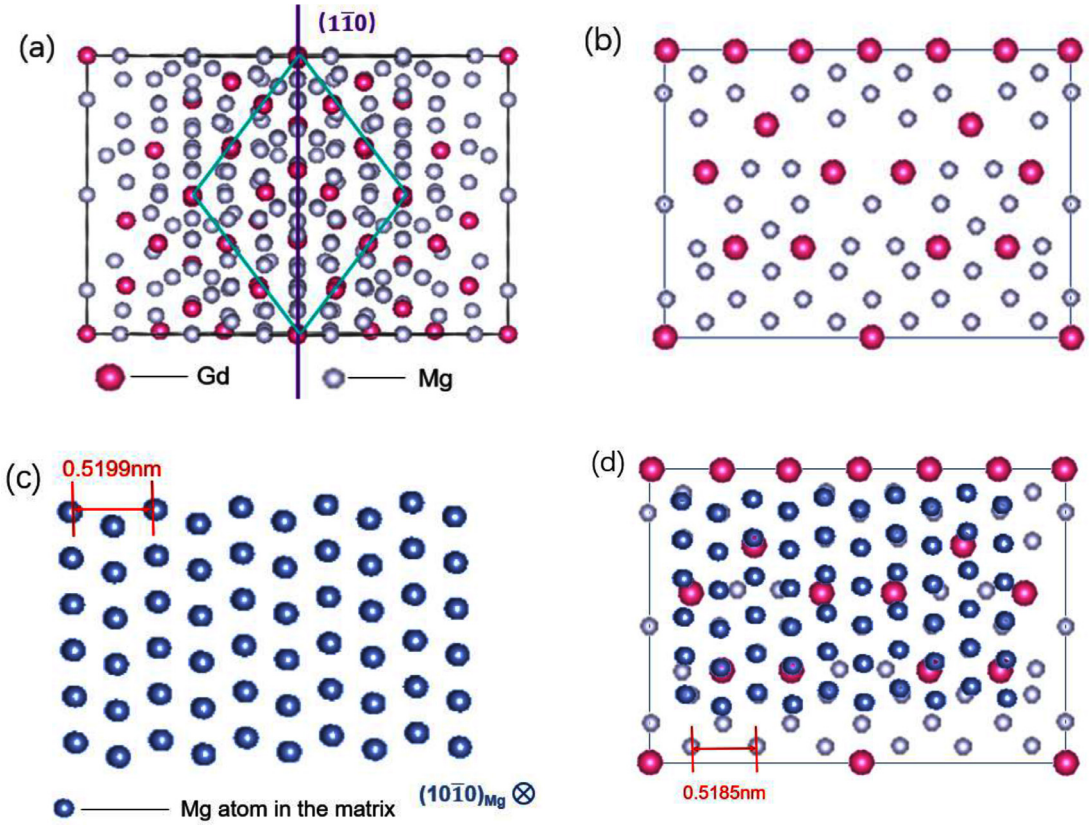

Fig. 3. (a) The long diagonal line of the "parallelogram" structure marked with blue lines is taken to obtain a cross-section of the atom shown in (b); (c) is the magnesium atomic plane of the matrix attached to the atomic plane in (b); (b) and (c) are superimposed to obtain (d); (e) the short diagonal line of the "parallelogram" structure marked with blue lines is taken to obtain a cross-section of the atom shown in (f); (g) is the atomic plane of the magnesium matrix connected to the atomic plane in (f); (f) and (g) are superposed to obtain (h) (For interpretation of the references to color in this figure legend, the reader is referred to the web version of this article).

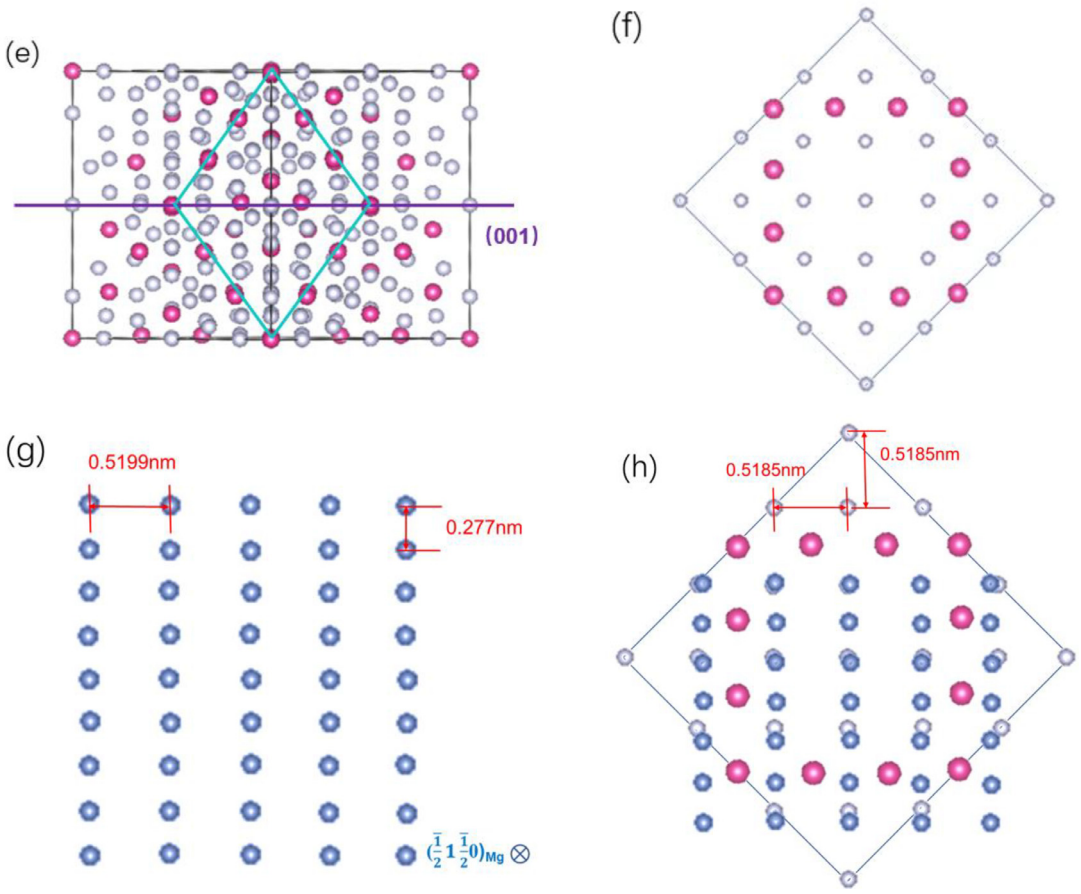

Fig. 3. Continued

matrix are in the left part of the hexagonal structure, which is also marked by a red square, as the β/Mg_2 interface in Fig. 4(b). However, the Gd atoms from the left view in the part of the Mg matrix have three atomic layers, which are marked with positions (A1, B1, C1) in Fig. 4(c) and (A2, B2 and C2) in Fig. 4(d). Therefore, the arrays of Gd and Mg atoms in the single line have 7 types, 111, 122, 112, 121, 211, 212 and 221 (number 1 instead of the Gd atom, number 2 instead of the Mg atom), in each structure. They correspond to layer1_1∼layer1_7 in the β/Mg_1 interface and layer2_1∼layer2_2 in the β/Mg_2 interface.

5. The calculation discussion

5.1. The separate energy

The symbol, W_{sep}, is utilized to measure the difficulty of the interface separation and then evaluate the interface stability. Generally, W_{sep} is the energy generated by separating the interface into two parts. W_{sep} is calculated as [18]:

$$W_{sep} = \frac{E_\beta + E_{Mg} - E_{interface}}{A} \quad (1)$$

Where E_β, E_{Mg} are the total energies of the Mg_5Gd, Mg bulk in the upper part and the other part of the interface. $E_{interface}$ is the energy of the interfacial structure. A is the interfacial area of the contact surface. W_{sep} is calculated by universal binding energy relation (UBER) [19]. The most stable structure has the largest absolute peak value. Thereby, these peaks will be compared with the corresponding relaxed structures to evaluate the possibility of existence.

Fig. 5 is the separation energies of these three structures. The separation energy of layer1_1 of the β/Mg_1 structure (absolute value: 2.89 J/m^2) is a bit higher than other layers. Similarly, layer2_1 (absolute value: 2.74 J/m^2) is also higher than others in the β/Mg_2 structure. The results show that the structure with the single-element atomic line may be more stable than others because different atomic arrangements decrease the system order which makes the system structure unstable. Therefore, Layer1_1 and Layer2_1 are the most stable structure in each interface.

Fig. 6 shows the two interfaces (β/Mg_1 and β/Mg_2) after relaxation, which are the most stable ones in every structural group. The thickness of this three-layer has changed from 7.66 Å to 6.82 Å in the β/Mg_1 interface, while shortened from 7.48 Å to 7.07 Å in the β/Mg_2 interface. And the thickness of the β/Mg_1 interface is more similar to the atomic thickness in Fig. 2(e) than the β/Mg_1 interface. The results show that the interface has the trend combined together and the bands of the interface in the β/Mg_1 interface may be stronger than other interfaces.

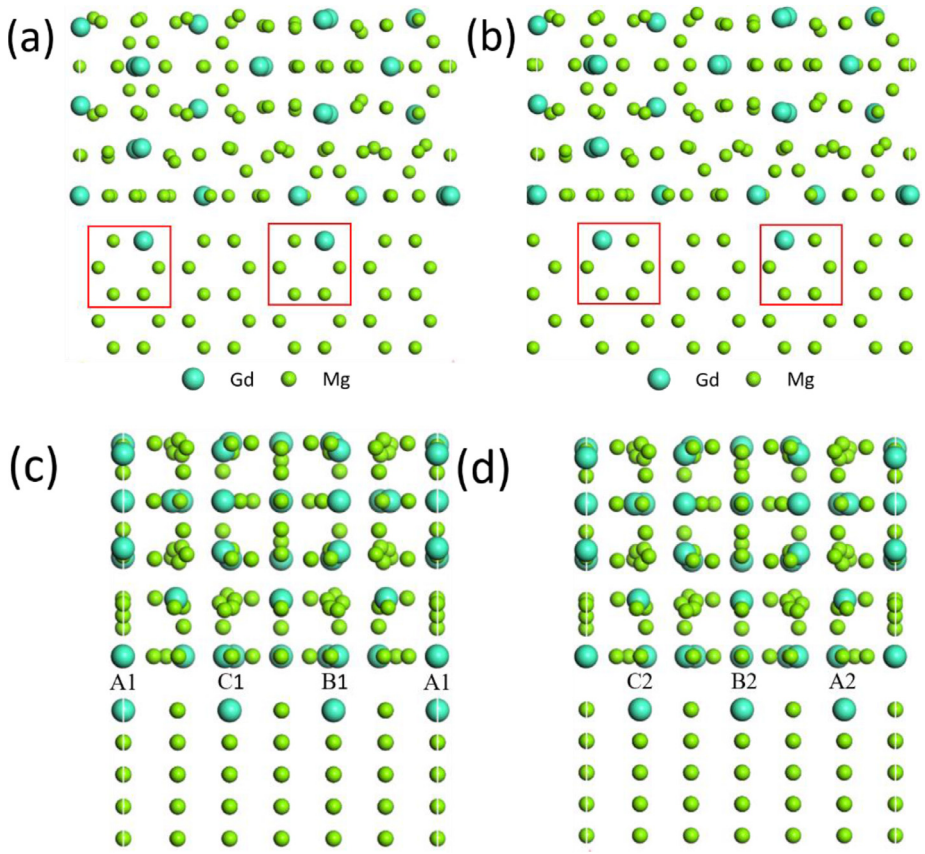

Fig. 4. Three possible structures: (a): β/Mg_1 structure; (b): β/Mg_2 structure; (c): the left view of β/Mg_1 structure; (d) the left view of β/Mg_2 structure (For interpretation of the references to color in this figure, the reader is referred to the web version of this article).

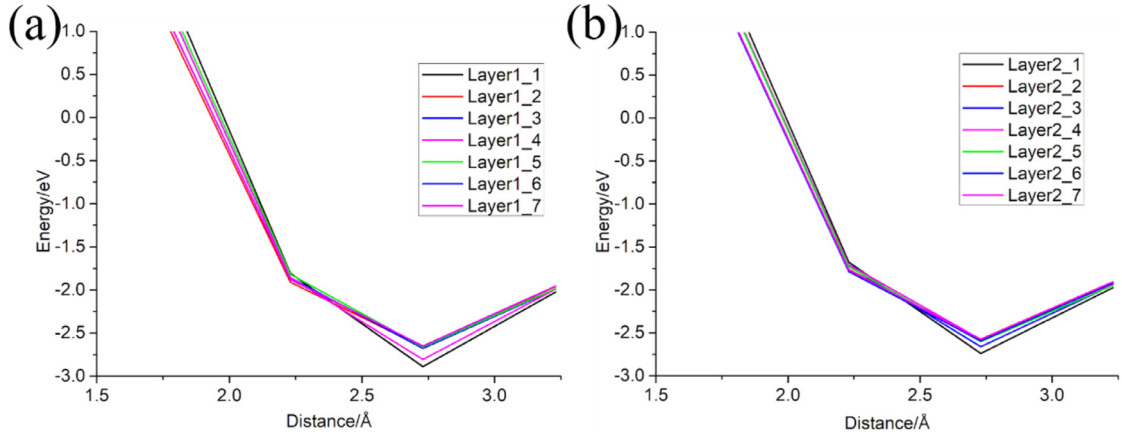

Fig. 5. The separation energies (W_{sep}) of (a) different β/Mg_1 structures; (b) different β/Mg_2 structures.

5.2. Interfacial energy

The interfacial energy is the structural energy of the interface between β and Mg matrix, which can evaluate the stability of the interfacial structure. The interface energy is given by thermodynamic equilibrium [20, 21]:

$$\gamma = \frac{E_{slab} - N_{Mg}\mu_{Mg}^{slab} - N_{Gd}\mu_{Gd}^{slab}}{2A} \quad (2)$$

where E_{slab} is the structural energy of the relaxed interface, A is the area of the cross-section interface, N_i and μ_i^{slab} are the number and chemical potential of each atom i in the interface structure, respectively (i = Mg or Gd).

While the chemical potential of bulk structure can be described as the total chemical potential of each atom, the chemical potential balances between the bulk and interface are given as:

$$\mu_{Mg_5Gd}^{bulk} = 5\mu_{Mg}^{slab} + \mu_{Gd}^{slab} \quad (3)$$

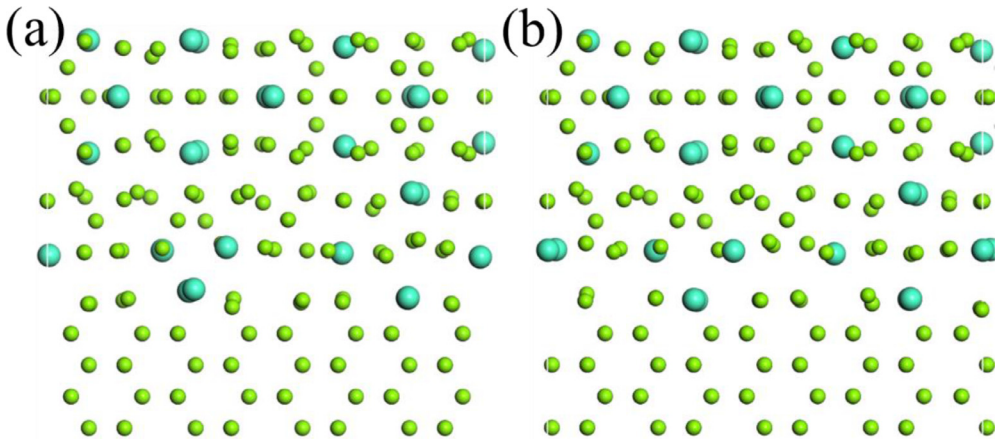

Fig. 6. The relaxed structures of the interface (a): β/Mg_1, (b): β/Mg_2.

Table 1
The different interfacial free energies.

Interface	E_{slab}/eV	N_{Mg}	N_{Gd}	A(Å^2)	γ/J•m^{-2}
β/Mg_1	−536.33	268	39	355.04	442.35
β/Mg_2	−533.82	268	39	354.10	443.77

$$\mu^{bulk}_{Mg_{matrix}} = \mu^{slab}_{Mg} \tag{4}$$

The final interface energy can be expressed as:

$$\gamma = \frac{E_{slab} - N_{Gd}\mu^{bulk}_{Mg_5Gd} - \left(N_{Mg} - 5N_{Gd}\right)\mu^{bulk}_{Mg_{matrix}}}{A} \tag{5}$$

After comparing interfacial energies of different structures in Table 1, the β/Mg_1 interface has a lower free energy (442.35 J/m^{-2}) than the interface β/Mg_2 (443.77 J/m^{-2}), which indicates that the β/Mg_1 interface is more stable than the other one. Therefore, it will probably be the possible structure of the layer compared with the β/Mg_2 interface. Moreover, the energy of this slab is also lower than the Mg_5Gd matrix (-177.09eV), which means there is an energy gradient in this interface with three atomic layer thicknesses. Therefore, the formation of the interface will be more possible.

5.3. Electronic characterization

The property of the interface structure always depends on the bonding strength, which greatly affects the phase stability. The bonding strength of these interfacial structures can be reflected through electronic characterization analysis, such as the charge density difference, the Mulliken population and the partial density of states (PDOS). The charge density difference shows the difference in charge transfer between interfaces, which will reveal the possible area of bond existence and then analyze the bonding strength. The Mulliken population is used to evaluate the charge transfer among atoms. Therefore, the bond strength of the interface will be analyzed by the difference of charge transfer between atoms and the change of bond length. The PDOS will indicate the classification of bonds intuitively. The overlap density of bonds will also reflect the bonding strength indirectly by bond distribution analysis.

Table 2
The Mulliken population.

Interface	ion	s	p	d	f	total	charge
β/Mg_1	Mg1	1.07	7.04	0	0	8.11	−0.11
	Gd1	2.48	6.35	1.21	7.77	17.81	0.19
	Mg2	1.02	7.13	0	0	8.15	−0.15
	Gd2	2.33	6.26	1.4	7.77	17.76	0.24
	Mg3	1.08	7.04	0	0	8.12	−0.12
	Gd3	2.48	6.36	1.19	7.76	17.78	0.22
	Mg4	1.02	7.38	0	0	8.4	−0.4
	Gd4	2.36	6.26	1.33	7.77	17.72	0.28
	Mg5	1.02	7.38	0	0	8.4	−0.4
	Gd5	2.35	6.25	1.33	7.77	17.71	0.29
β/Mg_2	Mg6	0.99	6.97	0	0	7.96	0.04
	Gd6	2.45	6.34	1.33	7.75	17.88	0.12
	Mg7	0.99	6.96	0	0	7.95	0.05
	Gd7	2.47	6.38	1.31	7.7	17.86	0.14
	Mg8	1.05	6.86	0	0	7.91	0.09
	Gd8	2.4	6.48	1.5	7.74	18.13	−0.13

Fig. 7 shows the charge density difference of interfacial structures. In Fig. 7(a), the positions of Gd and Mg atoms are marked in the image of charge density difference, which reveals that there are lots of charge transfers in the interface β/Mg_1. The atoms in the corresponding positions lost electrons if the color of spots is red (Gd), and get electrons if blue (Mg). Therefore, some ionic bonds will form between the atoms. However, the light color of atoms in the corresponding positions reveals that the bonds formed in the interface β/Mg_2 are different from the interface β/Mg_1 in Fig. 7(b). Mg atoms almost have the green color, while Gd atoms have the color of light red. And the area of red color is smaller than the interface β/Mg_1. The results reveal that there may be some metallic bonds formed between Mg and Gd atoms around the interface.

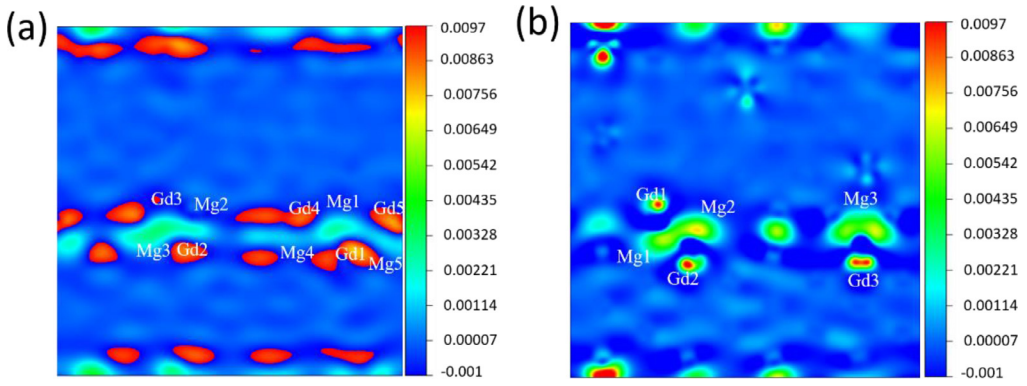

Fig. 7. The charge density difference of interfaces (a): β/Mg_1; (b): β/Mg_2(For interpretation of the references to color in this figure, the reader is referred to the web version of this article).

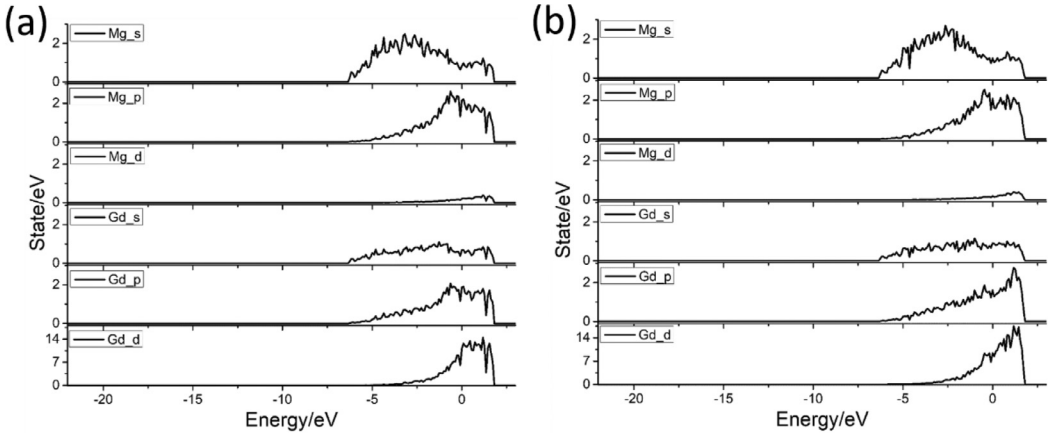

Fig. 8. The PDOS of interfacial structures (a): β/Mg_1; (b): β/Mg_2.

Table 2 shows the Mulliken population of these two interfaces. The β/Mg_1 interface has 5 groups of ion pairs, which indicates that Mg atoms will absorb electrons to become negative ions, while Gd atoms lose electrons to become positive. Therefore, the bonds between every group in the β/Mg_1 interface will probably be ionic bonds. The population between the second group (Mg2 and Gd2) is -0.42 and the length changes from 2.72 to 2.598, which reveals that the bond may be more stable and the interface has the tendency to approach each part. However, the interface β/Mg_2 just has 3 groups of ion pairs. Different from the interface β/Mg_1, most of the Mg atoms formed bonds in the β/Mg_2 interface will also lose electrons to become positive ions, while the Gd atoms also get electrons lost by other atoms. And there is just one group of ions with positive and negative ions. Therefore, bonds between bonding atoms will probably metallic bonds with weak ionic bonds. The largest population of them is 0.16 and the bond length changes from 3.112 to 2.964, which will also confirm it as the metallic bond. Moreover, the total charge transfer of ionic groups in the interface β/Mg_2 (Mg8/Gd8: 0.21) is smaller than the interface β/Mg_1 (Mg5/Gd5: 0.69) and the largest population of bonding atoms in β/Mg_2 is also smaller than β/Mg_1, which means that the bond in β/Mg_1 is stronger than that in β/Mg_2.

The PDOS of the possible interfaces with different atomic structures is shown in Fig. 8. The result indicates hybridization styles of different atomic levels. In Fig. 8(a), the hybrid area of Mg and Gd is almost in the range of -7eV $\sim$ 2eV, and these overlapping areas will reveal the formation trend of bonds. The p band of Mg overlaps the p and d bands of Gd in the range of -2eV $\sim$ 2eV, which shows strong ionic bonds may form in this structure. Moreover, the overlapping peaks of Mg-s, Mg-p, Gd-p and Gd-d in the range of 1eV $\sim$ 2eV prove the metallic bonds formed. Therefore, the bond of the β/Mg_1 interface is a combined bond of the strong ionic bond with the weak metallic bond.

For the β/Mg_2 interface in Fig. 8(b), the p band of Mg also overlaps the p and d band of Gd in the range of -2.5 eV $\sim$ 2eV, and the overlapping peaks are concentrated in the positive part. The results prove that the compound bond of the strong metallic bond with the weak ionic bond will dominate the interface.

6. Conclusions

Based on the analysis from atomic scale and the first principle study, the process of β phase growth and the hypothesis

of resultant β/Mg interfaces (β/Mg_1 and β/Mg_2) have been studied. The results indicate that:

(1) The rectangular β phase precipitates along the surface of the cylinder precipitate. The β in the aged 53h sample is more elongated than in the aged 4h sample, which strengthens the alloy.
(2) The β phase can be precipitated from the previously precipitated β phase, and the direction changes. The angle of change is approximately 125°. The β phase grows in steps when it is precipitated.
(3) At the edge of the β phase, there is a transition structure having a thickness of about three atomic layers, which consists of alternating triangles (three Gd atoms) and parallelograms (four Gd atoms). And the hypothesis of atomic structure is probably as the β/Mg_1 interface, which is more stable than other structures for the largest W_{sep}, lowest interface energy and the combined bonds of the ionic bond with the weak metallic bond.
(4) β' phase and β_H structure precipitate only at the edge of the length directions of β phase. The β' phase continues to grow into a β phase directly without the β_1 phase so that the length of the β phase increases.

Conflicts of interest

I would like to declare on behalf of my co-authors that the work described was original research that has not been submitted to any other journals, and is not under consideration elsewhere.

Acknowledgment

This work is financially supported by the National Natural Science Foundation of China (Grant No. 51825101) and the National Key Research and Development Program of China (Grant No. 2016YFB0701201). The authors gratefully acknowledge the support from Yang Zhao (Shanghai Jiao Tong University).

References

[1] C. Xu, T. Nakata, X.G. Qiao, M.Y. Zheng, K. Wu, S. Kamado, Sci. Rep. 7 (2017) 43391, doi:10.1038/srep43391.
[2] K. Wang, J. Wang, S. Huang, et al., Mater. Sci. Eng. A 733 (2018) 267, doi:10.1016/j.msea.2018.07.050.
[3] S.M. He, X.Q. Zeng, L.M. Peng, X. Gao, J.F. Nie, W.J. Ding, J. Alloy. Compd. 427 (2007) 316, doi:10.1016/j.jallcom.2006.03.015.
[4] R. Zhang, J. Wang, S. Huang, S. Liu, F. Pan, J. Magnes. Alloy. 5 (2017) 355, doi:10.1016/j.jma.2017.07.002.
[5] H.R.J. Nodooshan, W. Liu, G. Wu, et al., Mater. Sci. Eng. A 615 (2014) 79, doi:10.1016/j.msea.2014.07.056.
[6] J. Nie, Metall. Mater. Trans. A 43 (2012) 3891, doi:10.1007/s11661-012-1217-2.
[7] J. Zheng, Z. Li, L. Tan, X. Xu, R. Luo, B. Chen, Mater. Charact. 117 (2016) 76, doi:10.1016/j.matchar.2016.04.015.
[8] G. Kresse, J. Furthmüller, Comp. Mater. Sci. 6 (1996) 15, doi:10.1016/0927-0256(96)00008-0.
[9] G. Kresse, J. Furthmüller, Phys. Rev. B 54 (1996) 11169, doi:10.1103/PhysRevB.54.11169.
[10] G. Kresse, D. Joubert, Phys. Rev. B 59 (1999) 1758, doi:10.1103/PhysRevB.59.1758.
[11] T.J. Ma, Y.G. Li, W.Y. Li, Y. Zhang, D.G. Shi, A. Vairis, Mater. Charact. 129 (2017) 60, doi:10.1016/j.matchar.2017.04.008.
[12] J.P. Perdew, K. Burke, M. Ernzerhof, Phys. Rev. Lett. 77 (1996) 3865, doi:10.1103/PhysRevLett.77.3865.
[13] J.F. Nie, B.C. Muddle, Acta Mater. 48 (2000) 1691, doi:10.1016/S1359-6454(00)00013-6.
[14] D. Li, J. Dong, X. Zeng, C. Lu, Mater. Charact. 61 (2010) 818, doi:10.1016/j.matchar.2010.03.003.
[15] J.F. Nie, Scr. Mater. 48 (2003) 1009, doi:10.1016/s1359-6462(02)00497-9.
[16] X. Gao, S.M. He, X.Q. Zeng, L.M. Peng, W.J. Ding, J.F. Nie, Mater. Sci. Eng. A 431 (2006) 322, doi:10.1016/j.msea.2006.06.018.
[17] J.K. Zheng, R. Luo, X. Zeng, B. Chen, Mater. Des. 137 (2018) 316, doi:10.1016/j.matdes.2017.10.042.
[18] J.L. Du, Y. Fang, E.G. Fu, et al., Sci. Rep. 6 (2016) 1, doi:10.1038/srep33931.
[19] S. Shi, S. Tanaka, M. Kohyama, Phys. Rev. B 76 (2007) 1, doi:10.1103/PhysRevB.76.075431.
[20] Y. Jiang, J.R. Smith, A.G. Evans, Appl. Phys. Lett. 92 (2008) 1, doi:10.1063/1.2907339.
[21] F. Cao, J. Zheng, Y. Jiang, B. Chen, Y. Wang, T. Hu, Acta Mater. 164 (2019) 207, doi:10.1016/j.actamat.2018.10.045.